2.5 UAV NAVIGATION BY EXPERT SYSTEM FOR CONTAMINANT MAPPING

George S. Young*, Yuki Kuroki,, Sue Ellen Haupt
The Pennsylvania State University, University Park, Pennsylvania

1. INTRODUCTION

The intentional or unintentional release of a harmful atmospheric contaminant is a potentially devastating threat to homeland and defense security. Accurate identification of the source location and intensity is essential to predicting subsequent transport and dispersion of the contaminant. Insufficient spatial and temporal resolution of the available contaminant and wind-field observations make source characterization extremely difficult (Allen et al. 2006) when using typical networks of fixed sensors. Given sufficient observational data, however, the problem is feasible as shown by Long et al. (2008). That study demonstrated the use of the Gaussian puff equation as the dispersion model in identical twin numerical experiments applying a Genetic Algorithm (GA) to back calculate the required source characteristics solely from the observations on grids ranging from 8×8 to 2×2 of fixed location concentration sensors. It is not practical, however, to cover all societally important regions with a dense enough fixed sensor network to make that method practical. Therefore we study an alternative, the use of a mobile sensor system.

The coupling of concentration observations to dispersion model forecasts by a GA proved to be a fruitful way to determine both source characteristics and those of the transport and dispersion process. Using the Gaussian plume equation as the dispersion model, Allen et al. (2007a) applied a genetic algorithm to identify four parameters: source location (x,y), source strength, and wind direction. Even when noise was added to the concentration data to simulate the non-Gaussian nature of instantaneous turbulent dispersion, the results remain excellent for sensor grids of 8×8 and larger. That grid size presumes that the wind direction is unknown and requires receptors in all possible directions from a potential source. An earlier version of the model was validated with circular and spiral source array synthetic data configurations before being applied
to field test data from Logan, Utah (Haupt 2005) then was validated in the context of superimposed noise (Haupt et al. 2006). Allen et al. (2007b) extended that analysis with a more sophisticated dispersion model, SCIPUFF and correctly identified the time of release, source location, and apportioned contaminant contributions from multiple sources, even for concentration observations contaminated with moderate amounts of white noise as well as testing the model on field test data (Dipole Pride 26). Long et al. (2008) showed that the method can be extended to retrieve a total of seven parameters required for concentration field modeling: source strength, source location (x, y), puff centerline effective height, release time, transporting wind speed, and transporting wind direction. All of these studies required numerous fixed sensors to achieve successful source and meteorological characterizations. Deployment of fixed sensors at the required densities is not practical in many situations. Therefore, we explore the option of using a mobile sensor system based on unmanned aerial vehicles (UAV) that can be deployed in response to an alert issued by a single fixed sensor. The navigation system for such autonomous aircraft pose significant challenges because they must react in real time to the UAV's own observations to plan its future flight track.

Several approaches have been applied to this problem previously. Sporns and Lungarella (2006) showed that maximizing information structure is highly effective in generating coordinated behavior in mobile sensor platforms. Thus, they proposed the use of information theory to derive navigation instructions (i.e. waypoint list) for mobile sensors. In contrast, Singh and Fuller (2001) demonstrated a Model Predictive Control (MPC) scheme for navigating a vehicle with nonlinear dynamics through a vector of known waypoints to a goal while managing the constraints of UAV control. Such a system would serve as a second stage, implementing the navigation instructions as a series of UAV control commands. Here, we address only the first half of this problem, selection of waypoints defining transects to efficiently acquire the information required for source characterization. In contrast to that proposed by Sporns and Lungarella (2006), our navigation scheme is based on physics rather than statistics, taking advantage of a human-created expert system to reason from the UAV-observed morphology of the contaminant field. It is based on models of atmospheric transport and dispersion. This approach is demonstrated for both the Gaussian plume (continuous release) and puff (instantaneous release) models. For both situations, the expert system uses the observed contaminant distribution to plan the waypoints required for contaminant field tracking via the UAV. Therefore our UAV navigation system uses simple geometric reasoning rather than complex statistical calculations. Because our priority is gathering concentration data to back calculate the source characteristics, the mission is to provide both a rapid collection of the required data via wise selection of transect waypoints and a computationally efficient navigational system to achieve this selection. The resulting data are used by a GA-based source characterization scheme derived from that described by Long et al. (2008).

* *Corresponding author address:* George S. Young, The Pennsylvania State University, Department of Meteorology, 503 Walker Building, University Park, PA, 18802; e-mail: young@meteo.psu.edu

The goal of the UAV sampling trajectory is to obtain enough data to identify four parameters describing the release: source strength, source location (x, y), and wind direction. The could be used as an in-flight quality control parameter since the UAV would be equipped with both Global Positioning System (GPS) navigation and an airspeed sensor, so it could calculate the flight-level wind vector directly. The navigation and source characterization systems will be tested together in the synthetic environment of a set of identical twin experiments. Such a setup uses the same model to create the synthetic data as will be used to complete the back calculation. The identical twin configuration is not fully realistic because it assumes that the assimilating model has no error. In the real world no models are perfect, so the results of identical twin experiments are necessarily optimistic. The identical twin approach is, however, advantageous in that it lets us quantify the accuracy of the source characterization algorithm without contamination by model error. Thus, it is an ideal framework for developing and testing a new system. The system's limits are then characterized by superimposing noise on the synthetic concentration data.

2. PROCEDURES

2.1 *Genetic Algorithm*

A GA uses principals inspired by the fields of genetics and evolution to optimize the solution to a potentially non-linear problem (Holland 1975, Goldberg 1989, Haupt and Haupt 2004). It works by iteratively improving a population of trial solutions called chromosomes. Each chromosome is composed of the parameters that we seek to tune so as to optimize the output of some process. In this case we seek to optimize the fit between the modeled and observed concentration fields by tuning the wind direction, source strength and source location (x,y) used by the Gaussian dispersion model. The population of trial solutions is initialized with random values for each parameter that are distributed over the plausible range. A cost function measures the fitness of each trial solution, in this case the match between the modeled and observed concentration fields. Thus, following (Allen 2007b), the fitness of each chromosome is evaluated based on the following cost function:

$$\text{cost} = \frac{\sum_{\mathbf{t}=1} \sqrt{\sum_{\mathbf{r}=1}^{\mathbf{TR}} \left(\ln\left(\mathbf{aC_r} + \varepsilon\right) - \ln\left(\mathbf{aR_r} + \varepsilon\right)\right)^2}}{\sum_{\mathbf{t}=1} \sqrt{\sum_{\mathbf{r}=1}^{\mathbf{TR}} \left(\ln\left(\mathbf{aR_r} + \varepsilon\right)\right)^2}} \quad (1)$$

where C_r is the concentration predicted by the dispersion model, R_r is the concentration from observation r, TR is the total number of sensor observations, a and ε are constants used to minimize the impact of noise around the background concentration. This logarithmic form of the Root-Mean-Squared-Error (RMSE) allows useful information to be extracted from the low concentration fringe of the plume or the puff. The cost function is summed over all observations from both the UAV and a single fixed sensor that initially detects the contaminant, initiating the UAV flight protocol. The value of the normalization scale factor, a , is determined by taking the sum of every concentration value, R_r, over the entire domain and over all time steps and dividing the total by one. To avoid taking the natural logarithm of 0 for observations below the sensor threshold, a small offset ε (set to 1×10^{-13} in this study) is added to the scaled values of both observed and modeled concentration.

The GA updates the population of trial solutions by exchanging information between the fittest chromosomes of each generation (i.e., iteration). Each generation of trial solutions is sorted by cost function value. The GA used here is elitist and so retains the best candidate solution (Haupt and Haupt 2004). The rest of the next generation is created by mating the chromosomes via a rank-weighted roulette wheel selection (Haupt and Haupt 2004) where each chromosome is assigned a probability of mating based on its rank within cost-sorted population. The mating procedure blends each of the parameter values of two parent chromosomes to create two replacement (offspring) chromosomes. Following the mating process, a fixed percentage of the population is subject to mutation, replacing one randomly selected parameter value by a random number from the same range used to initialize the population. Mutation encourages a complete search of the solution space, preventing premature convergence to a local minimum. Haupt (2005) finds that large populations coupled with smaller mutation rates or small populations coupled with higher mutation rates lead to the most rapid convergence to the global optimum cost function value, thereby minimizing computational time by making the fewest possible cost function evaluations. The GA is generally adept at finding the correct fitness basin for the global optimum but somewhat slow in refining the trial solution to the actual optimum. Therefore it is followed by a more rapid gradient descent method that is efficient for searching the local fitness basin. The best candidate solution found by the GA after 100 iterations is thus used as the first guess for a Nelder-Mead downhill simplex algorithm (Nelder and Mead 1965), which performs a local search to find the minimum of that basin.

2.2 *Data handling*

Real world concentration data do not have the pure signal available in our synthetically constructed data. Typical situations involve both observational modeling errors that are absent from an identical twin experiment unless corrective steps are taken. In addition, for the Gaussian models used here there is an inherent mismatch between the ensemble average nature of the model predictions and the single realizations sampled by the sensor measurements. In our experiments we simulate the aggregate uncertainty by incorporating white noise into the observed concentration data. No

assumption is made concerning the source of this noise. Long et al. (2008) show the performance of the coupled model over a range of signal to noise ratios (SNRs) is similar for both additive and multiplicative noise. In our experiments we use Gaussian additive noise with a mean of 0 and a signal to noise ratio (SNR) of 5, a value in the middle of the range successfully tested by Long et al. (2008). For our study, we've used a clipped Gaussian additive noise: that is, noise-contaminated concentrations below 0 are set to 0 as would real world measurements of negative concentrations. Haupt et al. (2006) found little difference between results incorporating additive noise with those considering multiplicative noise.

2.3 *Concentration Modeling*

The Gaussian plume model is a time and ensemble averaged approximation to the true plume from a continuous point source. The Gaussian plume model is the particular solution to the eddy diffusion version of the advection/diffusion equation under the following assumptions that the conditions are steady state, the wind speed is constant with height, the eddy diffusivity is constant in space and time, and that mass is conserved.

Under these assumptions the Gaussian "point" source plume model is

$$\mathbf{C}(\mathbf{x},\mathbf{y},\mathbf{z}) = \frac{\mathbf{q}}{2\pi\mathbf{u}\sigma_y\sigma_z}\left[\exp\left(\frac{-(\mathbf{z}-\mathbf{h})^2}{2\sigma_z^{\,2}}\right)+\exp\left(\frac{-(\mathbf{z}+\mathbf{h})^2}{2\sigma_z^{\,2}}\right)\right]\left[\exp\left(\frac{-(\mathbf{y})^2}{2\sigma_y^{\,2}}\right)\right] \quad (2)$$

where C(x,y,z) is the pollutant concentration as a function of downwind position (x,y,z), u is the mean wind speed evaluated at effective release height h, q is the emission rate, and $\sigma_{y,}$ and σ_z quantify the lateral and vertical plume spread (with values that depend on downwind distance, x). The vertical spread is quantified as $\sigma_z = ax^b$. The horizontal spread is taken as

$$\sigma_y = \left(\frac{1000\mathbf{x}}{2.15}\right)(\tan\theta) \quad \text{where } \theta = \left(\frac{\pi}{180}\right)(\mathbf{c}-\mathbf{d}\ln(\mathbf{x})),$$

where x is in kilometers, $\sigma_{y,}$ σ_z are in meters, and θ is in radians (Beychok 1995). For neutral stability, a = 61.1, b = 0.9, c = 12.5 and d = 1.1 (Beychock 1995). The effective release height is h, includes buoyant rise of the plume near the source. The coordinate system is rotated such that the x-axis is along the direction traveled by the plume and the y-axis is the crosswind direction. The first exponential factor expresses the distribution of mass in the vertical dimension at a given downwind distance x, the first term signifying the initial release and the second denoting the virtual source due to reflection from the ground), while the second factor describes the distribution of mass in the crosswind dimension at a given downwind distance, x.

The release of a toxic contaminant is more likely to be an instantaneous release rather than a continuous emission. Therefore the Gaussian puff model is also tested. This model decouples the wind speed from the source strength so that we can back calculate both. In order to simulate a slightly less idealized environment, an asymmetric Gaussian puff is used as a crude approximation to a sheared puff. The Gaussian puff model is defined as

$$\mathbf{C}_r = \frac{\mathbf{q}\Delta\mathbf{t}}{(2\pi)^{1.5}\sigma_x\sigma_y\sigma_z}\exp\left(\frac{-(\mathbf{x}_r-\mathbf{ut})^2}{2\sigma_x^{\,2}}\right)\exp\left(\frac{-\mathbf{y}_r^{\,2}}{2\sigma_y^{\,2}}\right)\times \left[\exp\left(\frac{-(\mathbf{z}_r-\mathbf{H}_e)^2}{2\sigma_z^{\,2}}\right)+\exp\left(\frac{-(\mathbf{z}_r+\mathbf{H}_e)^2}{2\sigma_z^{\,2}}\right)\right] \quad (3)$$

where C_r is the concentration at receptor r, (x_r, y_r, z_r) are the Cartesian coordinates of the receptor relative to the source. q is the emission rate, Δt is duration of the release, t is the time since the release, u is the wind speed, (σ_x, σ_y, σ_z) are the standard deviations of the concentration distribution in the x-, y-, and z- directions, respectively.

The standard deviations of the model are computed according to Beychock (1994):

$$\sigma = \exp\left[I + J\ln(x) + K(\ln(x))^2\right] \quad (4)$$

where x is the downwind distance in km, and I, J and K are coefficients dependent on stability and can be found in Beychock (1994). We assume $\sigma_y = \sigma_x$.

2.4 *UAV Navigation Expert System*

The focus of this study is the development of an expert system for navigating a UAV through the data collection needed for source characterization for both continuous and instantaneous releases. The waypoint selection rules of these two expert systems are manually developed rather than statistically derived. Thus, each rule is based on geometric reasoning based on the UAV's own observations of the concentration field along with those from a single fixed sensor. Alternate rule systems are tested for the continuous release case while a single, considerably more complex, system is tested for the instantaneous release case.

The UAV navigation expert system is tested in a virtual environment. The simulated release is located at the center of a 1,400 m by 1,400m flight domain for the continuous release (plume) problem and at x = -6,000 and y = 0 in a 14,000 m by 14,000 m flight domain for the instantaneous release (puff) problem. These domain sizes reflect the advection distances for the contaminant during the time required for the UAV to map the concentration field adequately for the GA to back calculate the source characteristics. The speed of the wind transporting both plume and puff is set to 5 m/s, the wind direction is set to 270 degrees in meteorology coordinates (from the west), the UAV departure location is set to the least favorable location, an upwind corner of the flight domain: x = -700 m, y = 700 m for the continuous release and x = -7,000 m, y = 7,000 m for the instantaneous release. This is the most awkward position for both problems as it lies as far as possible from the plume or puff trajectory while still being located in the flight domain. The UAV speed is 20 m/s, a typical

value for small UAVs, but only four times the wind speed.

2.4.1 *Continuous Release*

We configure the simulation environment with a minimum of concentration sensors, one fixed surface-based sensor located randomly within the downwind half of the flight domain, i.e. somewhere downwind of the source. The flight domain is the area in which the UAV is allowed to operate. It includes the area to be protected, a city for example, and adequate surrounding airspace for the maneuvers described below. The other data collection component is an ensemble of expert-system driven autonomous UAV equipped to measure both concentration and the vector wind. The UAV are launched based on contaminant detection by the fixed sensor. Thereafter the expert system of each UAV works independently using information from both the fixed sensor and the UAV itself to navigate the autonomous UAV so as to collect sufficient data for source characterization and dispersion prediction. Figure 1 illustrates the navigation routes for the three candidate expert systems tested here. Each route in figure 1 corresponds to the track produced by the corresponding expert system. Each route is broken into straight passes separated by course and waypoints decisions made by the expert system.

The first pass of Route 1 is for the UAV to fly straight to the sensor and then to send the data to the GA for analysis. We optimize the source characteristics by applying the GA to the pass 1 data then calculate the route for the next pass using a single expert system rule. The pass 2 routing is calculated by

$$X_{aircraft} = \min(abs(X_{source} + 300), abs(X_{source} + X_{aircraft1})/2) \quad (5)$$

where $X_{aircarft}$ is the x component of the next waypoint, X_{source} is the source location as estimated by the GA and $X_{aircraft1}$ is the terminal waypoint of the first pass. For pass 2 the UAV flies upwind until it passes $X_{aircarft}$, then it progresses crosswind to transect the plume. After pass 2, the UAV again sends all available concentration data to the GA for recomputation of the source characteristics. At this stage in the flight approximately 150 concentration observations are usually available.

Route 2 differs from Route 1 in that the aircraft initially goes directly downwind until its x location exceeds that of the fixed sensor. Thereafter the UAV is governed by the same rules as in Route 1.

Route 3 begins with the UAV following the same track as Route 2 for pass 1. Pass 2, however, uses a different approach, because the GA optimization tends to fail if the distance between the aircraft track and the source location is too small. The expert system picks the waypoints for pass 2 using the following rule.

$$T = abs\left(\frac{x_{\text{int}} - x_{sensor}}{u_{aircraft} + u_{wind}}\right) \quad (6)$$

$$x_{pel} = T \times u_{wind} + x_{src} \quad (7)$$

$$d = abs\left(\frac{x_{sensor} - x_{src}}{2}\right) \quad (8)$$

$$dx = \left(\frac{x_{air} - x_{src}}{2}\right) \quad (9)$$

where T is the time taken by the downwind leg of pass 1, x_{int} is the aircraft x location after the pass 1 flight, x_{sensor} is the sensor x location, $u_{aircraft}$ is the UAV air-speed, u_{wind} is the wind speed, x_{pel} is the distance to which the plume extends by the end of pass 1, x_{src} is the GA-optimized source, *d* is half the difference between the sensor x location and the optimized source x location, *dx* is half the difference between the original aircraft x location and the GA-optimized source x location, and x_{air} is the x location of the UAV at the end of pass 1. If x_{pel} is larger than *d,* pass 1 is deemed to be as close to the source as is useful, so the aircraft shifts downwind for pass 2. If not, the aircraft shifts upwind. When the UAV has flown along wind by a distance dx_t, it turns crosswind to complete pass 2. Example flight tracks for route 1 and route 3 are shown in figure 2 along with the corresponding UAV-sampled concentration values.

2.4.2. *Instantaneous Release*

The task of the expert system is more complex for an instantaneous release because the concentration field is evolving with time as the puff drifts downwind and disperses. Thus, the aircraft needs first to find the puff and then to maneuver to keep passing through the puff as it drifts downwind. A single expert system was designed to do this by evaluating the time-dependent concentration records from both the UAV and fixed sensor. The expert system launches the UAV as soon as the fixed sensor detects the puff and then maneuvers the UAV to make multiple passes through the estimate of the center of the moving puff.

As with the expert system for Route 1 for the continuous release scenario, the pass 1 rule of the instantaneous release expert system is that the UAV fly directly toward the sensor. The pass 2 rule selects one of two patterns. If the heading angle for pass 1 is between 180° and 315°, counter-clockwise relative to downwind, pass 2 follows pattern 1 in which the UAV flies northward for distance Δy then goes upwind. This leg thus takes the UAV along the track followed by the estimated puff center. Under any other circumstance the UAV follows the 2 rule pattern (figure 3) in which the UAV heads north for distance *N* then turns through angle ϕ. To solve for ϕ, four conditions are required.

$$t_{aircraft} = \frac{N + \sqrt{n^2 + a^2}}{u_{aircraft}} \quad (10)$$

$$t_{puff} = \frac{\Delta x - a}{u_{wind}} \tag{11}$$

$$\sin\theta_1 \sin\phi + \cos\theta_1 \cos\phi = 0 \tag{12}$$

$$\frac{N - n}{\Delta x} = \tan\theta_1 \tag{13}$$

$$\frac{\Delta x - a}{n} = \tan\phi = \tan\theta_2 \tag{14}$$

where $\Delta x = x_{aircraft} - x_{max}$, $x_{aircraft}$ is the x component of the last location of pass 1. x_{max} is the x location of the pass 1 maximum concentration observation, θ_1 is the heading flown on pass 1, $u_{aircraft}$,and u_{wind} are the UAV speed and wind speed respectively. N, n, a, ϕ are defined as shown graphically in Figure 3. Pattern 1 is designed to collect enough information to make a firm decision on the track of the puff center while Pattern 2 is designed to intercept the puff given definitive information on the track of the puff center.

Pass 3 to pass 6 all use the same navigation rule because we already have a tentative puff location based on information from pass 1 and pass 2. The task of passes 3 to 6 is to refine the puff location. Thus the UAV is navigated by the estimated puff location. The puff track is estimated from the points of maximum concentration along the previous passes. In contrast to a plume, however, the puff presents a moving target. Otherwise the UAV navigation is similar to the plume Route 3. An example flight track is shown in figure 4.

2.5 *Statistical Analysis Methods*

The expert system UAV navigation systems described above usually work well given concentration data from a single sensor and the UAV. In same cases, however, the GA fails to characterize the source adequately. For both continuous and instantaneous releases the back calculation can fail for sensor locations that do not provide adequate samples of the contaminant. Even in these trying circumstances the GA-expert system combination often works. Therefore, to overcome these challenges we adopt the technique of launching an ensemble of non-communicating UAV, each of which tries to solve the source characterization problem on its own. The ensemble size is called $N_{aircraft}$. The "typical" answer from the ensemble is taken as the system's result, eliminating most outliers. Both the mean and median operators are tested to see which best eliminates outliners. The statistical results presented will be the average and standard deviation of the 100 Monte Carlo runs, each of an ensemble of $N_{aircraft}$ UAVs. The number of ensemble members (i.e. independent UAVs) was varied from 4 to 50. Results will be shown for each of these fleet sizes.

3. RESULTS

3.1 *GA Tuning*

A sensitivity study was conducted to determine which combination of GA parameters yields accurate source characterization with minimum computational cost. When we move to more refined dispersion models, we expect the computation of the concentration field to be computationally expensive, so we wish to determine the best combinations of population size and mutation rate to minimize the number of calls to the cost function and hence to the dispersion model. This is a Pareto multi-objective optimization problem. That is we are trying to minimize both error and pseudo-runtime, competing objectives. We expect a "front" of solutions. This analysis is similar to that undertaken by Haupt et al. (2007). We note that, the GA convergence depends on the number of iterations. Since the solution is known for these identical twin experiments, we can stop the GA when the error reaches a pre-specified tolerance level, in this case 1 percent of source strength. We wish to explore a wide range of parameter combinations. The goal is to minimize the number of cost function evaluations required to reach this level in an effort to minimize the CPU time. Mutation rates examined are 0.01, 0.02, 0.04, 0.08, 0.16, and 0.32. Population sizes are 10, 20, 40, 80, 160, 320, 640 and 1280. Iteration counts are 10, 20, 40, 80, 160, 320, 640 and 1280. Each point in the plotted results represents the mean of 100 Monte Carlo runs. Figure 5 shows that the larger the pseudo-runtime (iteration count times population size), the smaller the magnitude of the errors. We wish to minimize the CPU time, however, so we pick the three combinations of population size and iteration count having the potential for combining high accuracy and low runtime. These are tested more thoroughly to determine the optimum mutation rate.

Figure 6 shows the results for the 3 population sizes and iteration counts suggested by Figure 5. As before, each calculation is repeated 100 times and the results are averaged to minimize the stochastic uncertainty. The four best configurations were reevaluated with 1000 trials to select the final configuration. From these results we conclude that one of the best combinations is population size 40, mutation rate 0.32, and iteration count 640. For these 1000 test runs it produces source strength error magnitude larger than 50% only 10 times (1% of the cases).

To quantify our confidence in the ability of the GA-optimized coupled model methodology to match a known solution, a Monte Carlo technique is used. The GA is run on the same problem 100 times with different initial random seeds. From the resulting sample of solutions we are able to estimate the mean, median, and standard deviation of the error distribution. An experiment with 1000 runs shows that the mean source strength error is 0.15, median source strength errors is 0.12 and standard deviation source strength error is 0.17 for population size 40, iteration count 640, and mutation rate 0.32. The actual emission rate is q -= 1

kg/s. The error is $abs(q_{act} - q)$, q_{act} is actual concentration, and q is back calculated concentration.

Table 1 shows the results of a similar test conducted with a randomly specified wind direction and source location. The first metric used here, w_mean, is the mean difference in wind direction over the 100 Monte Carlo runs between the actual value and the ensemble mean of the back calculated values. Std stands for the corresponding Monte Carlo standard deviation. The second metric, w_median, is similar except that it is based on the ensemble median. Its corresponding Monte Carlo standard deviation is also reported. These quality analyses are repeated for the other back calculated parameters, q_ indicates the source strength errors while x_ and y_ indicate source location coordinate errors. These results indicate that it is difficult to back calculate the source location when the true source is near the edge of the domain, particularly when part, or all, of the plume immediately advects or disperses out of the domain. To avoid this problem the UAV flight domain should focus on the area to be protected, so that sources near the crosswind and downwind boundaries are not a threat. Thus, for all subsequent tests we fix the true source location at (0, 0), the maximum threat location. In contrast, a source at (30,-590) that lies near the edge of the flight domain is a difficult position to back calculate, although the ensemble method improves the results. The plume from such a source would not, however, cross the area to be protected.

To explore the utility of the GA-based source characterization method to real world problems, we must also consider the impact of sensor dynamic range, again via identical twin experiments. Following Long et al. (2008) we test with an 8×8 grid that has 64 sensors. In this study, however, a detectability threshold is applied to mimic the behavior of real world sensors. This threshold is expressed in terms of the dynamic range of concentrations sampled, i.e. the maximum of the sensor reported concentrations times a specified dynamic range scale. Any values less than this threshold are set to zero. Table 2 shows the results for an eight member ensemble for each threshold value in a logarithmic scale. These results imply that we require at least 13 sensors to exceed the threshold value in order to achieve accurate results. For an 8x8 sensor array, meeting this condition requires a sensor threshold scale of 10^{-11}, an unrealistic value for a real sensor. Therefore in the next section we pursue the single sensor situation with a realistic threshold scale of 10^{-3}. The additional data points required for a successful back calculation are acquired using mobile sensors as described above.

3.2 *Continuous Release*

A virtual autonomous aircraft is used as the mobile concentration sensing platform as described in section 2.4.1. We first try Route 3 for sensor SNR=5 and ensemble size of 4, 10, 20 and 50. Figure 7 shows how the ensemble method improves back calculation of wind direction and source characterization. Route 3 produces accurate results if we set the fixed sensor location at least 30 m from the source x location. This constraint is realistic because we don't need to find the source if the sensor is very near the source, because the extreme concentrations will suffice to localize the source as being in the immediate vicinity of the sensor. Route 1 does not have this near-field problem but does not produce solutions as accurate as Route 3. The Route 1 computing times are slightly shorter than those for Route 2. Route 1, however, requires at least 20 ensemble members to obtain accurate results, the same as for Route 2, while Route 3 produces a successful back calculation with only four ensemble members. Analysis of the UAV tracks requested by these three expert systems explains why these differences occur. The plume penetrating leg of Route 1 is asymmetric relative to the plume axis, while that for Route 3 is symmetric. Moreover, accurate back calculation of the source characteristics requires two UAV passes through different parts of the plume. Failure to achieve plume penetration at two well separated locations limits the amount of independent information available and so degrades the accuracy of the GA calculation. Route 1 also exhibits problems if the fixed sensor is located very near the edges of the flight domain. Increasing the ensemble size does not improve this situation and sometimes makes it worse. Therefore, the expert system rule set for Route 3 is the best choice of those tested.

3.3 *Instantaneous Release*

Back calculating the source characteristics for an instantaneous release proved to be more difficult than was the case for a continuous source because of the time dependence of the concentration field and the challenge of locating the moving puff from the limited data provided by one fixed concentration sensor and another aboard the UAV. The moving target issue also requires that the flight domain for an instantaneous release be increased in size by an order of magnitude, to a 14 km square. For the ensemble sizes tested here the method often has a problem quantifying the crosswind location y. This problem might be ameliorated by using the UAV-GPS-measured wind direction in the Gaussian concentration model rather than forcing the GA to derive both wind direction and y location. This change would eliminate the potential for cross-talk between these two parameters during the back calculation. Baring this change, Table 3 suggests that 20 ensemble members are required to yield a reliable solution for an instantaneous release, in contrast to the continuous release results where the best route required only four. Likewise, for an instantaneous release the UAV-plus-GA system requires at least passes through the puff to back calculate the source characteristics accurately, where as for a continuous release two well-placed passes through the plume sufficed.

As noted above, the crosswind source location is hard to back calculate accurately for an instantaneous source. In contrast, accurate back calculation of the source strength, wind direction and x location is easy.

We analyze this difference using the histogram of the back calculated y component of the source position. Figure 8 indicates that the ensemble method works for 95% of the cases, but in the remaining 5% has a problem with crosswind location. The instantaneous release version of the UAV navigation system combines elements from continuous release Routes 1 and 3 because we must first find the puff, then track it for long enough to document both its motion and its rate of expansion. Figures 4 and 8 imply that we can back calculate the source characteristics if we get at least three well separated passes through the core of the puff, although this often requires a total of six pass attempts.

3.4 *Discussion*

The tests described above demonstrate that we can use a UAV to obtain enough data for the back calculation of source characteristics provided we are given warning by a single randomly placed fixed sensor to stimulate launching the UAV. These results suggest that use of a small ensemble of UAVs would allow us to work with a much smaller number of fixed sensors than would typically be required to characterize a source. This approach could potentially yield large cost savings compared to siting a large number of fixed sensors.

Our navigation system is based on a human-created expert system using geometric and physical reasoning based on wind speed and direction and the locations where the UAV passes through concentration peaks. In contrast, previous UAV navigation methods for source location have used Neural Networks or other complex biologically-based theories (see Sporns et al. 2006). Our simple expert system method obtains an answer both accurately and quickly. The computational complexity of the method is low. For example, the back calculation for an 8×8 grid of fixed sensors requires more computational time and provides less accuracy than our UAV method. The Gaussian plume model problem is relatively easy to back calculate accurately, while the puff model exhibits a 5 % error rate on back calculation of the crosswind location.

4. CONCLUSIONS

Source characterization using the Gaussian plume and puff models optimized via a GA is tested using identical twin experiments incorporating additive noise into the synthetic data. An expert system is developed for navigating autonomous aircraft in such a manner that concentration data collected by the virtual UAV improves the characterization skill. In contrast to previous studies that required an 8×8 grid of fixed sensors for this task our expert system allows back calculation of source characteristics with a single fixed sensor and a small fleet of UAVs. This means we may apply our strategy in those real world problems where dense fixed sensor networks are impractical.

When we detect a release with the single sensor, the expert system navigated autonomous aircraft are launched into the virtual world of the identical twin experiment to collect concentration data. This information is then used to back calculate source strength and location as well as the wind direction. The latter is used as a check on the system as the parameter is also available from the UAV's GPS and air-speed systems. From this information we can back calculate the source characteristics both precisely and quickly using a Genetic Algorithm. Use of an ensemble of UAV launches minimizes the error in this back calculation and yields accurate estimates of source strength for the plume model for two plume-symmetric flight legs with just four ensemble members. In contrast, for the puff model, twenty ensemble members and six flight legs are required to provide sufficient information to back calculate the source location.

Our results have been validated using an identical twin experiment approach to construct the synthetic data for use with virtual UAV. While such an approach is ideal for algorithm testing purposes, future work should test our model and expert system with actual unmanned airplane and field test data. Also using multiple UAVs to track the contaminant in a coordinated fashion could help avoid computational limits and acquire data in more a timely manner to compensate for the tight time constraints inherent in emergency management.

Acknowledgements: The second author was supported by Japan Ground Self Defense Forces during this study. The authors thank to John Wyngaard, Kerrie Long, Andrew Annunzio, Anke Beyer-Lout, and Luna Rodriguez for insights and advice.

References

Allen, C.T., G.S. Young, and S.E. Haupt, 2007a: Improving Pollutant Source Characterization by Optimizing Meteorological Data with a Genetic Algorithm, *Atmos. Environ.,* **41**, 2283-2289.

Allen, C.T., S.E. Haupt, and G.S. Young, 2007b: Source Characterization with a Receptor/Dispersion Model Coupled With A Genetic Algorithm, *Journal of Applied Meteorology and Climatology,* **46**, 273-287.Beychock, M. R., 1994: Fundamentals of Gas Stack Dispersion, 3rd ed. Milton Beychock, pub., Irvine, CA, 193 pp.

Beychok, M.R., 1995: *Fundamentals of stack gas dispersion*. 4rd Edition, California, USA, p. 50 – 56.

Daley, R., 1991: Atmospheric Data Analysis Cambridge University Press, New York, NY, 457 pp.

Haupt, R.L., and S.E. Haupt, 2004: *Practical Genetic Algorithms*, *Second Edition with CD*, John Wiley and Sons, New York, NY, 255 pp.

Haupt, S.E., 2005: A Demonstration of Coupled Receptor/Dispersion Modeling with a Genetic Algorithm. *Atmos. Environ.,* **39**, 7181-7189.

Haupt, S.E., G.S. Young, and C.T. Allen, 2006: Validation of a Receptor/Dispersion Model with a Genetic Algorithm Using Synthetic Data. *J. Appl. Meteor.* **45**, 476-490.

Haupt, S.E., G.S. Young, and C.T. Allen, 2007: A Genetic Algorithm Method to Assimilate Sensor

Data for a Toxic Contaminant Release, *Journal of Computers*, **2**, 85-93.

Haupt, S.E., R.L. Haupt, and G.S. Young, 2008: A Mixed Integer Genetic Algorithm used in Chem-Bio Defense Applications, *Journal of Soft Computing,* accepted.

Krysta, M., M. Bocquet, B. Sportisse, and O. Isnard, 2006: Data Assimilation for Short-Range Dispersion of Radionuclides: An Application to Wind Tunnel Data. *Atmos. Env.* **40**, 7267-7279.

Long, K.J., S.E. Haupt, and G.S. Young, 2008: Optimizing Source Characteristics and Meteorological Data for a Contaminant Release with a Genetic Algorithm, submitted to Optimization and Engineering.

Lungarella, M., and Sporns, O. 2006: Mapping information flow in sensorimotor networks. PLoS Comp. Biol. **2**, 1301-1312.

Pasquill, F., 1961: The Estimation of the Dispersion of Windborne Material. *Meteor. Mag.*, **90**, 33-49.

Singh, L. and Fuller, J, 2001: Trajectory generation for a UAV in urban terrain, using nonlinear MPC. American Control Conference, **3**, 2301-2308

Sporns, O. and Lungarella, M. 2006: Evolving coordinated behavior by maximizing information structure. In Rocha, L. et al. (eds.) Proc. of the 10th Int. Conf. on Artificial Life.

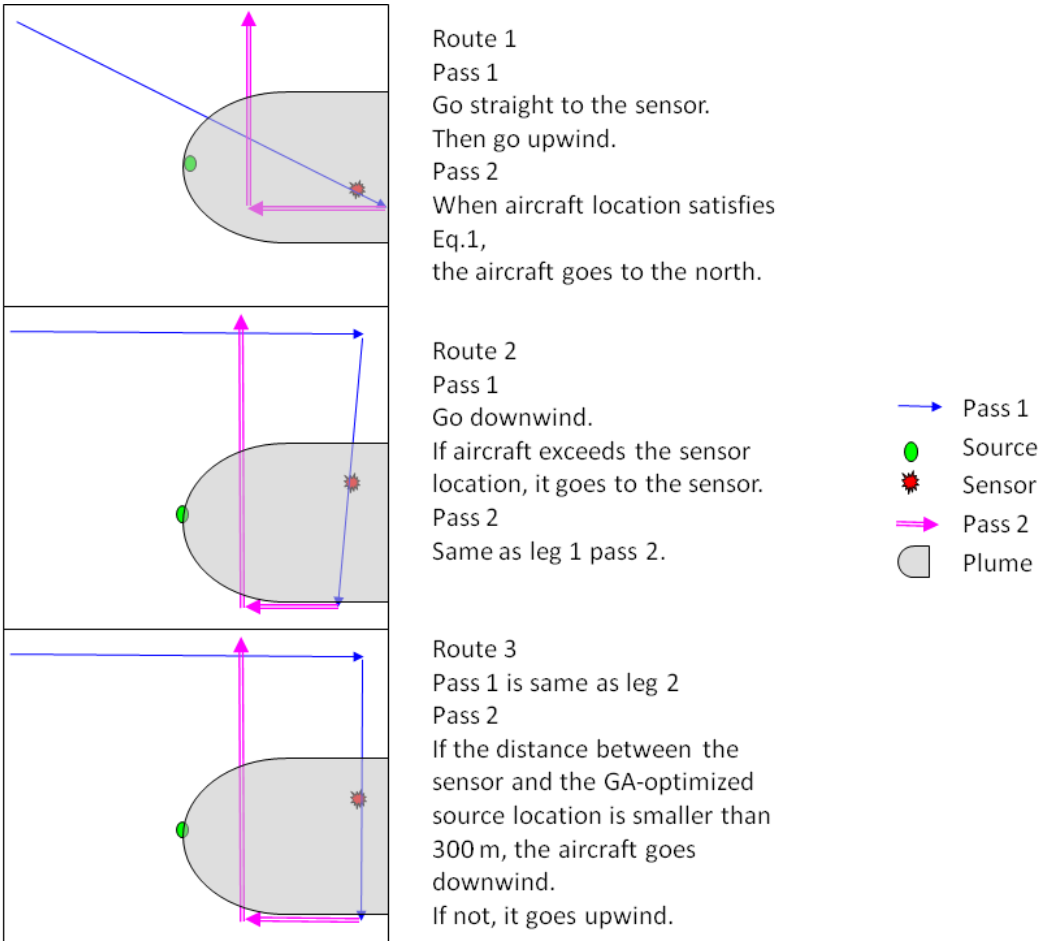

Figure 1. Sample UAV routes for the three candidate UAV navigational expert systems for continuous release characterization.

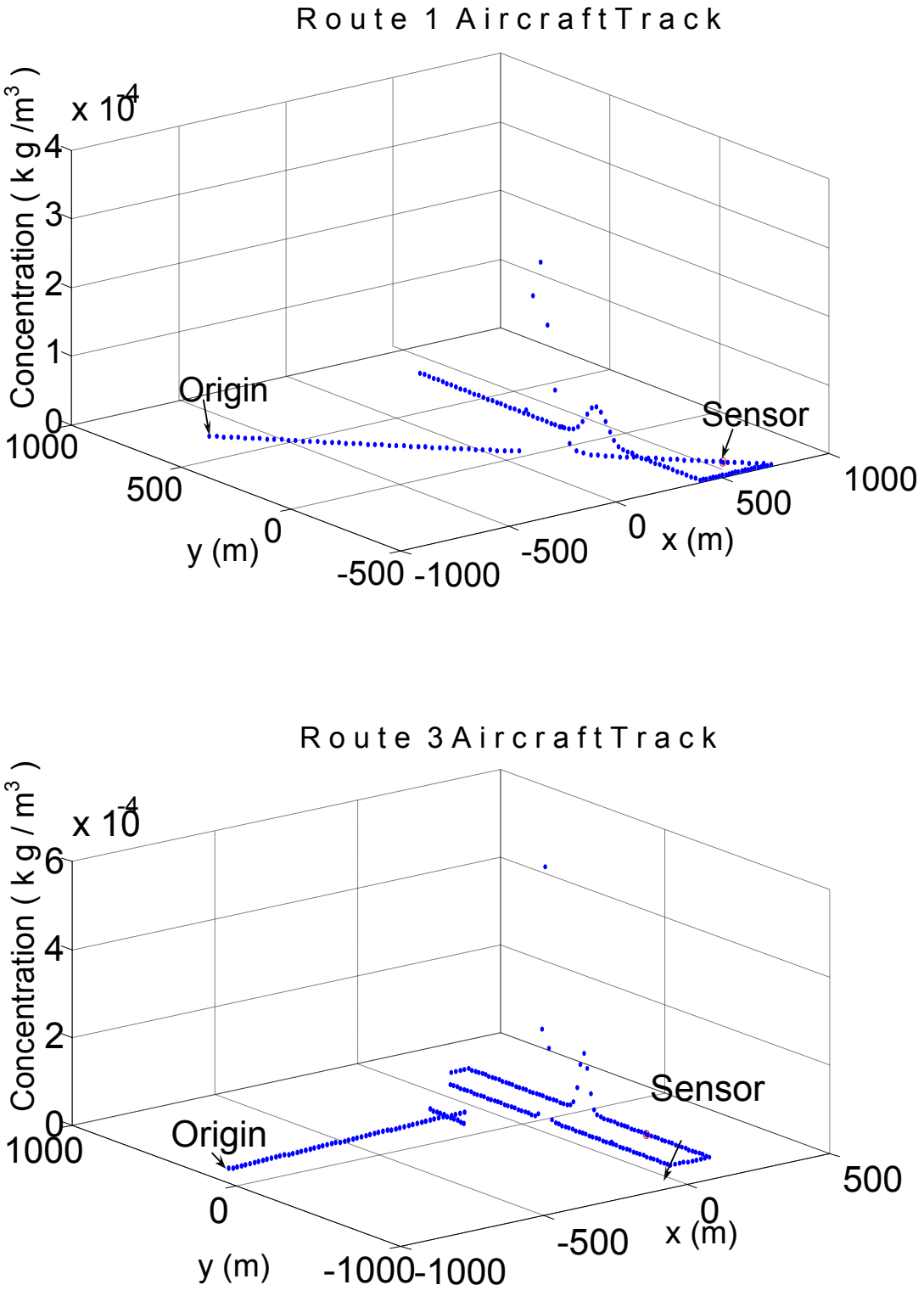

Figure 2. Sample flight tracks for Route 1 and Route 3 plume characterization expert systems. The horizontal axes are: x represents along wind and y the crosswind directions. The vertical axis is concentration as sensed by the UAV.

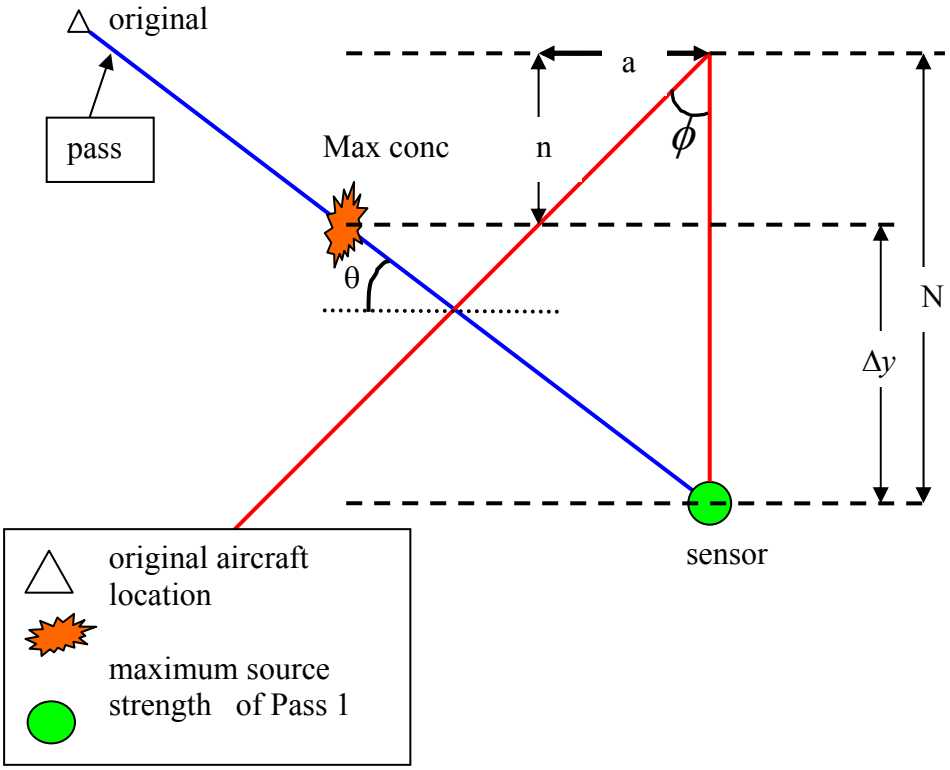

Figure 3. Pass 2 rule for Puff source characterization. Variables shown on the figure are the inputs for equations 10 through 13.

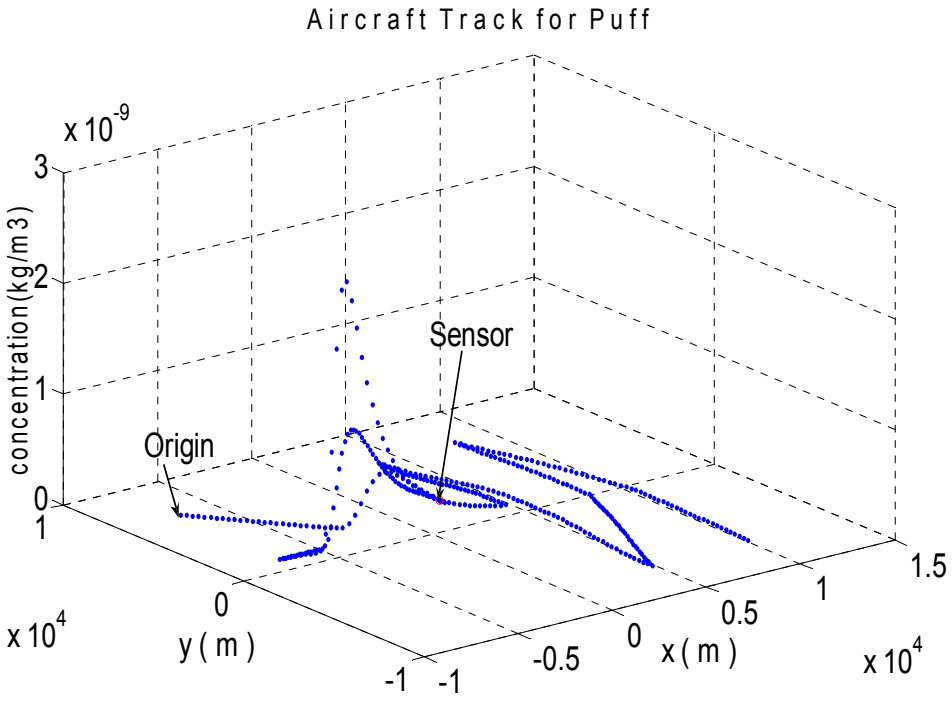

Figure 4. A sample flight track for the puff scenario. The concentration shows as three Gaussian transects on the early legs of the flight. Subsequently the puff disperses enough to be less apparent on the diagram. The axes are the same as for Figure 3.2.

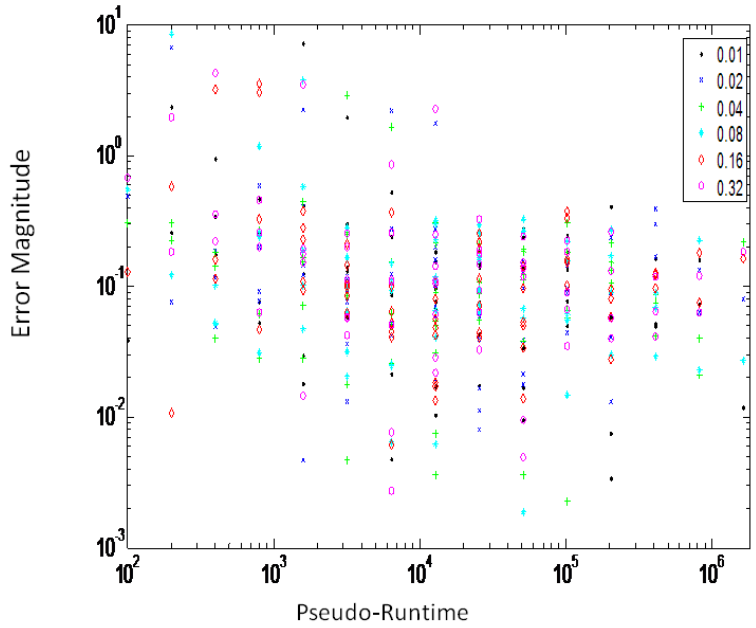

Figure 5 Monte Carlo mean accuracy versus pseudo-runtime results for 362 combinations of the GA parameters. The pseudo-runtime is the population size times the iteration count. The source strength accuracy is measured because it is the most difficult aspect of the plume source characterization problem.

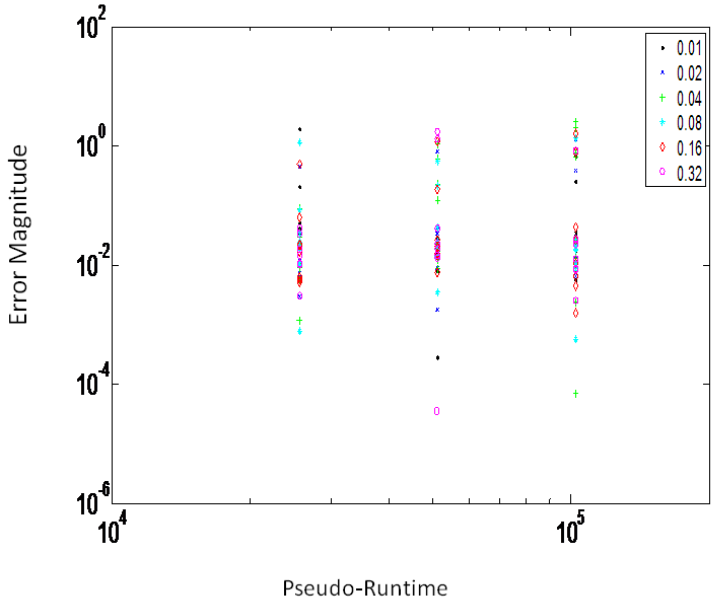

Figure 6 Same as Figure 5, but showing the mean of 1000 runs for the three best combinations of the GA parameters.

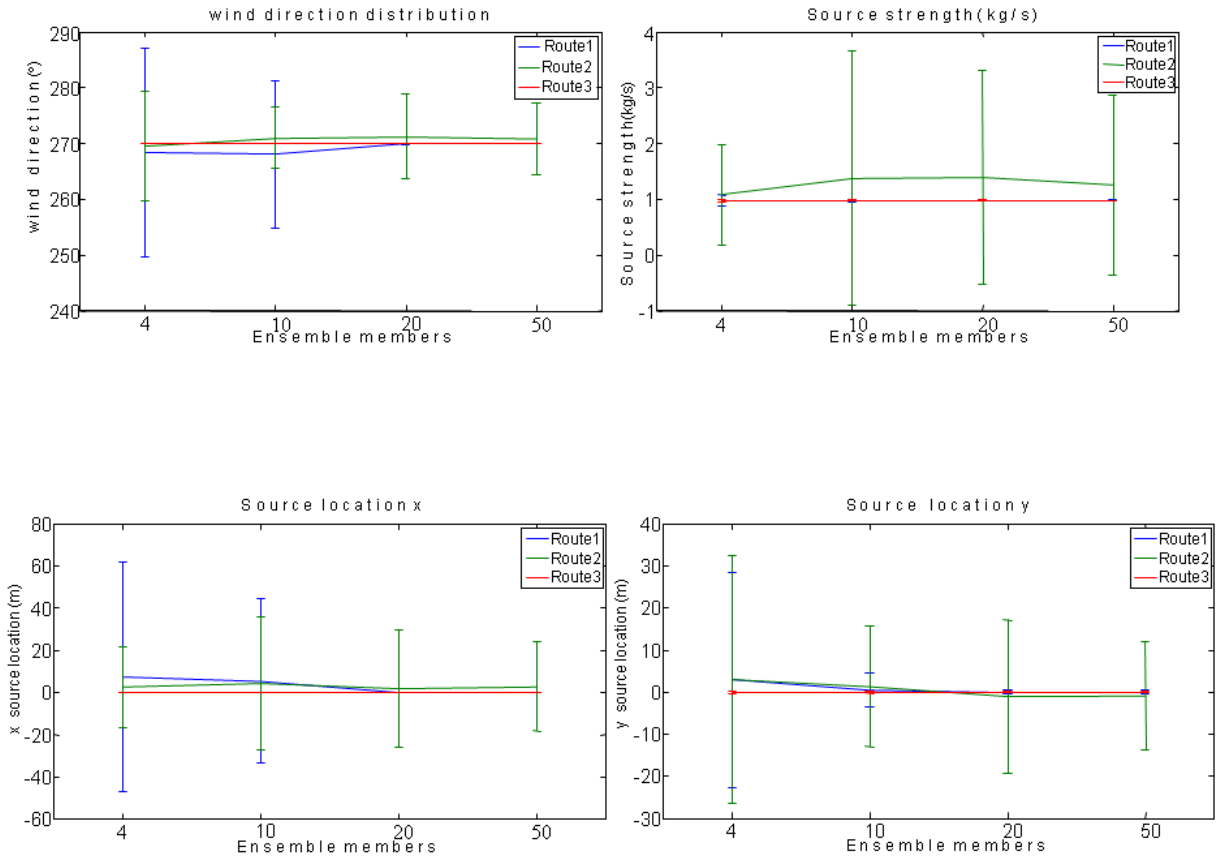

Figure 7 Plume source characterization result as a function of UAV route. Blue color is Route 1, green is Route 2, and red is Route 3. Horizontal axis represents each ensemble member. Error bars indicate the standard deviation. Actual solutions are that the wind direction is 270°, the source strength is 1 kg/s, and source location (x,y) = (0,0).

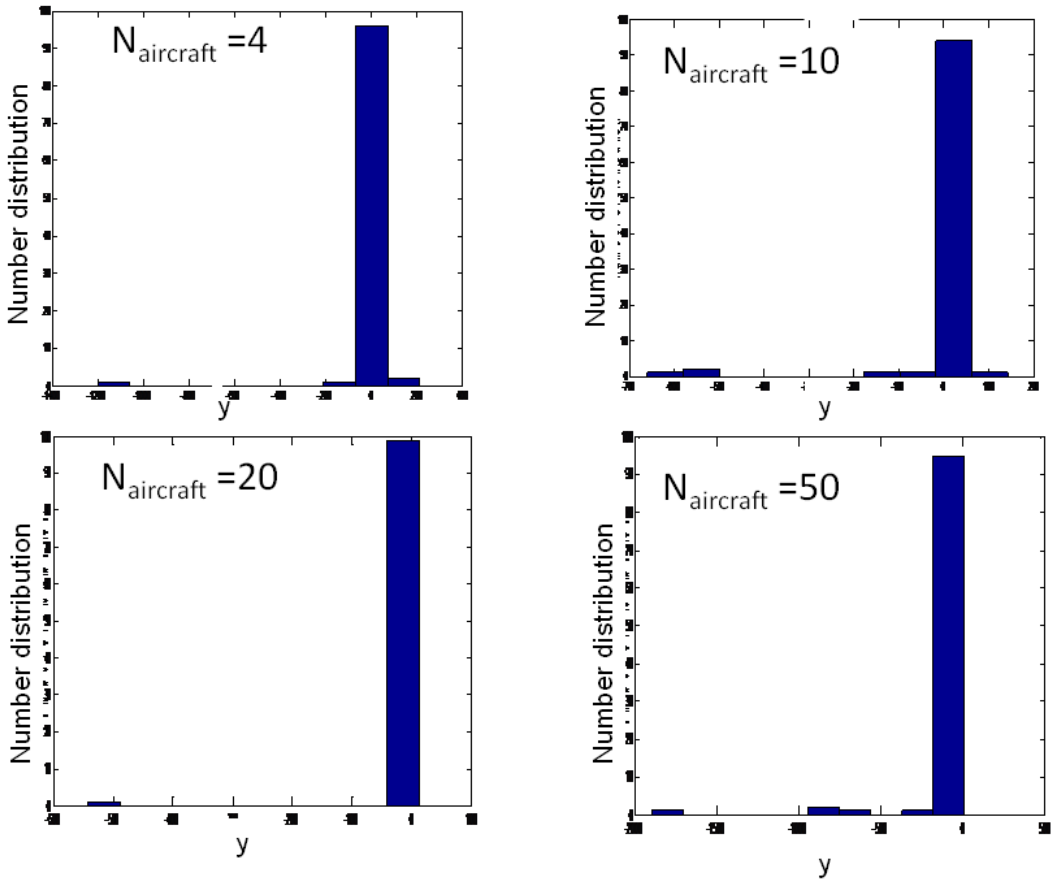

Figure 8. Histogram of the crosswind y distribution for various ensemble sizes in the puff source

Table 1. The statistical results for random source location and wind direction. All statistics are computed over 100 Monte Carlo runs. The column headings are defined in the text.

Ensemble member	w_mean	std	w_median	std	q_mean	std	q_median	std
4	11.23	39.58	9.81	42.78	2.672	44.22	0.73	3.35
6	11.00	36.21	9.40	38.79	1.60	19.03	0.51	1.18
8	10.27	35.76	8.94	42.11	5.16	135.87	0.58	2.31
10	12.19	39.94	10.60	46.22	3.71	65.49	0.56	2.67
12	9.13	32.61	7.56	38.89	0.81	3.67	0.43	0.85
14	7.97	28.06	5.68	29.48	507.33	1.60E+04	0.47	1.41
16	10.68	34.12	8.30	39.54	10.89	312.84	0.55	2.00

Ensemble member	x_mean	std	x_median	std	y_mean	std	y_median	std
4	14.22	38.04	13.30	36.57	13.71	34.06	12.79	34.13
6	13.15	32.81	11.67	33.00	14.73	44.20	13.27	46.14
8	13.72	44.10	12.88	47.10	11.59	33.32	10.66	32.89
10	15.15	47.25	14.20	48.15	14.84	49.93	13.06	49.57
12	12.16	35.81	11.34	39.03	12.83	48.61	11.55	48.08
14	12.92	38.95	10.97	40.61	12.60	35.96	10.61	35.00
16	15.25	51.55	13.75	51.21	15.38	45.80	13.97	47.62

Table 2. The statistical results for an ensemble of eight members as a function of threshold scale. Column headings are as in table 4.1. Nthresh is the number of the sensor above the threshold.

threshold scale	w_mean	std	w_median	std	q_mean	std	q_median	std
0	0.080	0.21	0.049	0.037	0.13	0.17	0.11	0.091
1.00E-01	4.48	0.087	4.50	0.041	3.26	0.15	3.15	0.026
1.00E-02	4.47	0.11	4.49	0.041	3.31	0.17	3.15	0.030
1.00E-03	0.63	0.042	0.63	0.047	7.37	0.39	7.38	0.43
1.00E-04	1.24	0.038	1.24	0.047	5.55	0.24	5.54	0.29
1.00E-05	1.77	0.59	2.31	0.48	1.24	0.79	1.80	0.47
1.00E-06	3.06	0.46	2.95	0.033	0.95	0.31	0.98	0.089
1.00E-07	0.64	0.045	0.64	0.059	0.67	0.10	0.67	0.10
1.00E-08	0.64	0.047	0.64	0.054	0.66	0.098	0.65	0.10
1.00E-09	0.64	0.050	0.65	0.056	0.67	0.090	0.67	0.10
1.00E-10	0.14	0.37	0.050	0.031	0.18	0.30	0.12	0.088
1.00E-11	0.076	0.20	0.044	0.034	0.12	0.16	0.11	0.096

x_mean	std	x_median	std	y_mean	std	y_median	std	Nthresh
0.88	2.51	0.49	0.37	0.70	1.09	0.60	0.45	64
41.50	0.54	41.58	0.36	111.67	0.44	111.78	0.25	7
41.42	0.78	41.56	0.35	111.55	0.63	111.76	0.29	7
18.05	0.33	18.02	0.37	117.43	0.27	117.42	0.31	8
13.37	0.43	13.36	0.50	83.58	0.39	83.55	0.46	9
23.28	6.93	29.73	6.08	43.25	8.53	40.75	6.6	10
24.89	5.40	23.66	0.36	26.66	2.90	26.32	0.49	11
2.07	1.14	1.98	0.63	0.671	0.67	0.63	0.53	12
2.06	1.13	1.94	0.55	0.70	0.62	0.65	0.46	12
1.96	0.53	1.99	0.56	0.65	0.45	0.70	0.50	12
1.60	4.40	0.51	0.37	1.04	1.88	0.66	0.46	13
0.78	2.37	0.42	0.32	0.59	0.99	0.51	0.41	13

Table 3. Puff results for various ensemble sizes. Each column is headed with the true value and contains the mean and standard deviation of 100 Monte Carlo runs. w is the wind direction, q is source strength, while x and y define the source location.

Ensemble	270		1		-6000		0	
members	w	std	q	std	x	std	y	std
4	269.95	0.71	1.00	0.16	-6000	10.34	-9.81	124.46
10	269.90	0.56	0.98	0.040	-6000	7.43	-17.45	99.66
20	269.96	0.31	0.98	0.023	-6000	3.28	-5.60	54.38
50	269.75	1.29	1.01	0.21	-6000	8.09	-43.78	230.86